RSC Advances

ROYAL SOCIETY OF CHEMISTRY

www.rsc.org/advances

RSC Advances

ARTICLE

Versatile Hierarchical Cu/Fe_3O_4 Nanocatalysts for Efficient Degradation of Organic Dyes Prepared by Facile, Controllable Hydrothermal Method

Received 00th January 20xx,
Accepted 00th January 20xx

DOI: 10.1039/x0xx00000x

www.rsc.org/

Zhenzhen Wang, Shangru Zhai,* Jialing Lv, Haixin Qi, Wei Zheng, Bin Zhai and Qingda An*

A novel monodispersed hierarchical nanocomposite catalyst of Cu/Fe_3O_4 was successfully synthesized through a short-time (just 4 h), facile, eco-friendly one-pot hydrothermal method. The as-prepared Cu/Fe_3O_4 nanocomposite was well characterized and the results showed that the products were spherical in morphology with diameter of about 100 nm. The BET surface area of the nanospheres was 37.16 m^2/g, indicating that the product showed a porous character, and the major BJH pore size was 3.73 nm. The saturated magnetization of the Cu/Fe_3O_4 nanospheres was 48.0 emu g^{-1}, which facilitate their separation and recovery with the aid of an external magnet. In addition, the influences of experimental parameters such as the dosage of trisodium citrate dehydrate (Na_3Cit) and urea as well as reaction duration time were investigated in detail to fully elucidate the formation mechanism. More charmingly, the Cu/Fe_3O_4 nanocomposites exhibited excellent catalytic activity towards the reduction of hazardous organic dyes (4-nitrophenol, 4-NP; congo red, CR; methylene blue, MB) in aqueous medium in the presence of $NaBH_4$ with very fast kinetics and good stability. The relationship between Cu precursor addition amount and catalytic ability was also established. Considering the simplicity of operation procedure, short time, low cost as well as easy recycling of the catalyst, this preparation protocol may shed light on the fabrication of other metal oxides materials; and hopefully, this hierarchical nanocomposite may find potential applications in other domains like heavy metal removal or antibacterial.

Introduction

Dyes and pigments that contain heterocyclic aromatic compounds as well as nitro aromatics are generally present in the waste waters from various industries, such as textiles, printing, leather, petrochemical, and pharmaceutical industries, etc.[1-3] On the one hand, strong colour of dyes and pigments not only results in serious esthetic problems to the contaminated aquatic ecosystem but also leads to ecological problems.[4] On the other hand, they are carcinogenic and mutagenic in nature.[5-8] More troubling, they can escape from conventional wastewater treatment processes and persist in the environment because of their hydrophilic nature, high stability against light, temperature, water, chemicals and not biodegradable property.[9,10] Hence, the effective removal of these type environmental threats is vital of importance. All kinds of wastewater treatment techniques, such as Fenton-like reactions,[11] photocatalysis,[12-17] biological degradations,[18] and adsorption,[19,20] etc., have been applied to the treatment of dye-containing effluents. However, most of these methods suffer from some disadvantages or limitations, such as harsh working pH ranges, secondary pollution, expensive post-process, limited application scale, and unthoroughness. Thus far, prominent research progress has been made in the chemoselective reduction of aromatic nitro compounds using H_2 with the aid of heterogeneous catalysts.[21] Amongst them, catalytic hydrogenation of various dyes with $NaBH_4$ as the hydride source has been assumed to be an important, safe, and green alternative route,[22,23] but the reduction cannot be achieved or need longer time in the absence of specific catalyst.[24,25] Thus, there is urgent demand of fabricating a heterogeneous catalytic material for the efficient degradation of aromatic dyes.

In the last few years, nanoscale metal particles (especially noble metal nanoparticles, NPs) have attracted widespread research interests due to their charming and specific optical, electronic, catalytic properties and wide applications in the field of microelectronics, data storage, antibacterial, drug delivery, bioimaging, and catalysis, etc.[26,27] In particular, a significant change in reduction potential for metal NPs in comparison to bulk metals, due to the more negative Fermi potential, allows them to act as the ideal catalysts in various electron transfer processes.[28] Taking the practically catalytic application into account, metal NPs are commonly immobilized onto all kinds of supports so as to reduce the

Faculty of Light Industry and Chemical Engineering,
Dalian Polytechnic University,
Dalian 116034, P. R. China.
E-mail: zhaisr@dlpu.edu.cn
anqingda@dlpu.edu.cn
† Footnotes relating to the title and/or authors should appear here.
Electronic Supplementary Information (ESI) available: [details of any supplementary information available should be included here]. See DOI: 10.1039/x0xx00000x

higher surface energy as the result of small size and thus avoid the aggregation and decrease of catalytic activity.[29-31] For example, Mignani et al.[8] supported Ag NPs onto commercial polyethyleneimine-functionalized silica beads as catalyst for the decoloration of MB and other azo dyes in the presence of excess $NaBH_4$. Gao et al.[32] applying plasma-assisted synthesis method immobilized Ag NPs into 3D mesoporous cellular foams (MCFs) of silica and used for the reduction of 4-NP. Ghosh et al.[33] prepared Cu NPs loaded mesoporous silica SBA-15 catalysts and used them to catalytically reduce various dyes with the help of excess $NaBH_4$. Additionally, Ag NPs was also well dispersed onto SBA-15 and exhibited fascinating catalytic performance for the reduction of 4-NP reported by Naik et al.[34] Even though the problem of aggregation of metal nanoparticles can be efficiently resolved, the sophisticated, difficult, energy-consuming and costly traditional isolation and recovery techniques, e.g. filtration, centrifugation are normally used, which limit their practical applications. In this context, simplification of synthetic procedure and utilization of easy separation and recovery method or support materials were the two urgent problems needing to be further improved.

The magnetic materials have recently emerged as an alternative to conventional support materials in catalysis because of their unique magnetic separation property and inherent high thermal and mechanical stability.[35,36] Combining the advantages of magnetic materials and metal NPs to fabricate a promising catalyst opens new possibilities for the achievement of desirable catalytic activity and effective magnetic separability. So far, several methods have been developed to prepare the magnetically recyclable catalysts. However, the typical fabrication procedure of these composite materials can be divided into four stages. Firstly, the magnetic component was pre-synthesized by conventional coprecipitation method or solvothermal procedure. Subsequently, they will be modified or functionalized by inert SiO_2, carbon layers, functional organic groups, specific polymers or biomass. Thereafter, desired metal ions were deposited onto their surface through electrostatic, complex or chemical interactions. Finally, these as-anchored metal ions were in situ reduced by hydrazine, $NaBH_4$, or dimethyl formamide, which are strong and hazardous reducing agents.[37-39] Undoubtedly, these preparation procedures are multi-step, cockamamie, time-consuming and environmentally unfriendly. In light of these disadvantages, much effort has been made to seek to facile, effective, environmentally friendly, and safe synthesis technologies for the preparation of magnetic metal nanocatalysts. Recently, one-pot synthesis method of magnetic composite catalytic materials has become a particularly important object of research, and has attracted a growing interest because of its simplicity and availability. Ai et al.[28] prepared Ag-Fe_3O_4 composite catalyst based on the one-step ethylenediamine (EDA)-assisted solvothermal process and they exhibited excellent catalytic activity, convenient magnetic separability, and long-term stability for Rhodamine B (RhB) reduction. Zhang et al.[40] reported one-pot fabrication of Ag-Fe_3O_4 nanocomposites using $AgNO_3$ and $FeCl_3$ as precursors and EG as reductants. Wang et al.[41] systhesized Cu doped Fe_3O_4 (Fe_3O_4:Cu) particles via solvothermal pathway for the adsorption of arsenic. In our previous work, employing the novel one-pot synthetic route, we also successfully fabricated Fe_3O_4/Cu composite catalysts with ethylene glycol as solvent and reductant.[22] However, despite these outstanding achievements on the one-pot synthesis methodology, the preparation process was always related to organic solvents (e.g. EG), and the reaction time was usually beyond 12 h. Therefore, it should be of particular importance to explore low-cost, time-saving, green, straightforward, and large-scale production methods for the synthesis of magnetically recyclable catalysts.

Herein, we for the first time presented a one-pot hydrothermal method to fabricate Cu/Fe_3O_4 nanocomposite catalysts with water as green solvent, urea as alkali source, and Na_3Cit as biocompatible electrostatic stabilizer as well as reductant. It was worth noting that the fabrication process was carried out in aqueous solution, without using harmful reagent, surfactant or organic solvent; additionally, the nanocomposite catalyst could be obtained with very short react time (only 4 h), which indicated a promising, short-time, facile, green, and cost-effective synthesis method for large-scale synthesis of hierarchical Cu/Fe_3O_4 nanocomposite catalysts.

Experimental section

Chemicals Ferric chloride hexahydrate ($FeCl_3{\cdot}6H_2O$) was obtained from Tianjin Kermel Chemical Reagent Factory, China. Trisodium citrate dihydrate (Na_3Cit), copper nitrate trihydrate ($Cu(NO_3)_2{\cdot}3H_2O$), congo red (CR), and methylene blue trihydrate (MB) were purchased from Sinopharm Chemical Reagent Co., Ltd., China. Urea was gained from Shenyang New West Reagent Plant. 4-Nitrophenol (4-NP) and sodium borohydride ($NaBH_4$) were supplied by Aladdin Chemistry Co., Ltd., China. All chemicals were analytical grade and used as received. De-ionized water was used throughout the experiment.

Preparation of Cu/Fe_3O_4 nanoscomposites Hydrothermal fabrication of hierarchical Cu/Fe_3O_4 was carried out as follows: $FeCl_3{\cdot}6H_2O$ (3.7 mM), Na_3Cit (0, 1.7, 3.4, 5.1, 6.8, 8.2 mM), urea (0, 3.3, 6.6, 10.0, 13.3 mM) and $Cu(NO_3)_2{\cdot}3H_2O$ (0.1, 0.3, 0.5, 0.7, 1.0, 1.3 mM) were dissolved into 80 mL de-ionized water under magnetic stirring at room temperature. After stirring, the resulting clear solution was transferred into a 100 mL Teflon-lined stainless-steel autoclave to heat at 200 ^{o}C for a certain time, and thereafter cooled naturally to room temperature. Then, the precipitate was gathered and washed by de-ionized water for many times with the aid of a magnet and finally vacuum-dried at 60 ^{o}C for 12 h. The as-obtained magnetic Cu/Fe_3O_4 nanocomposite with initial dosage of Cu precursor varied from 0.1 mM to 1.3 mM was marked as $Cu_{0.1}/Fe_3O_4$, $Cu_{0.3}/Fe_3O_4$, $Cu_{0.5}/Fe_3O_4$, $Cu_{0.7}/Fe_3O_4$, $Cu_{1.0}/Fe_3O_4$, and $Cu_{1.3}/Fe_3O_4$, respectively. The Cu/Fe_3O_4 nanocomposite in the article refers to $Cu_{1.0}/Fe_3O_4$ unless otherwise noted. For comparison, the pure Fe_3O_4 nanospheres and Cu were also synthesized under the identical condition.

Evaluation of catalytic property and versatility of Cu/Fe_3O_4 nanocatalysts The catalytic property and versatility of the as-prepared Cu/Fe_3O_4 nanospheres were carefully investigated through the degradation of different organic dyes i.e. the catalytic decolorization of 4-NP, CR, and MB in the presence of excess $NaBH_4$ at room temperature. The typical catalytic reaction process was provided as follows: 0.7 mL dye aqueous solution (5 mM/L for 4-NP, 1mM/L for CR and MB), 17 mL de-ionized water, and 1.3 mL freshly prepared $NaBH_4$ aqueous solution (0.2 M/L) were mixed in a three-necked flask under nitrogen atmosphere, followed by the addition of 1 mg/mL Cu/Fe_3O_4 aqueous solution (1.0 mL for 4-NP, 0.5 mL for CR and MB). As the catalytic reaction proceeded, the color of the corresponding solution faded gradually in time and the catalytic activity was monitored by UV-Vis spectrophotometer at the maximum adsorption peaks of dyes (400 nm for 4-NP, 498 nm for CR, 665 nm for MB).

Stability and reusability testing of Cu/Fe_3O_4 nanocatalysts The leaching test was performed to inspect the stability of active ingredient in the nanocomposite. After reaction for 1 min, the solid catalyst was separated from the reaction system by magnetic separation and the filtrate obtained was continuously stirred under the same reaction condition.

The recyclability of the catalyst was also investigated by consecutive reusing the catalyst. After the reduction of dyes was achieved, the catalysts were collected from the mixture by a magnet, washed with de-ionized water and then dried for the next cycle. This procedure was repeated for 6 times.

Characterization X-ray diffraction (XRD) patterns were recorded by a Shimadzu XRD-6100 diffractometer with CuKα radiation (λ = 1.54060 Å) from 10^o to 80^o at 5^o min^{-1} scanning speed. Field emission scanning electron microscopy (FESEM, JSM-7800F electron microscope, JEOL, Japan) and transmission electron microscopy (TEM, JEM-2000EX electron microscope, JEOL, Japan) were applied to characterize the morphology and size of the as-prepared samples. The surface elemental composition was obtained by X-Max50 energy dispersive X-ray analyzer (EDS, Oxford, UK) in the form of pressed pellets and selecting all the area in the field of the electron microscope. X-ray photoelectron spectroscopy (XPS) measurements were carried out using the Thermo Scientific ESCALAB250 spectrometer (Thermo VG, USA) with monochromatic AlKa radiation (1486.6 eV). Magnetism was analyzed by Lake Shore 7410 vibrating sample magnetometer (VSM) at room temperature. UV-Vis absorption spectra were recorded on a Agilent Cary 60 spectrophotometer.

Results and discussion

Characterizations of Cu/Fe_3O_4 nanospheres

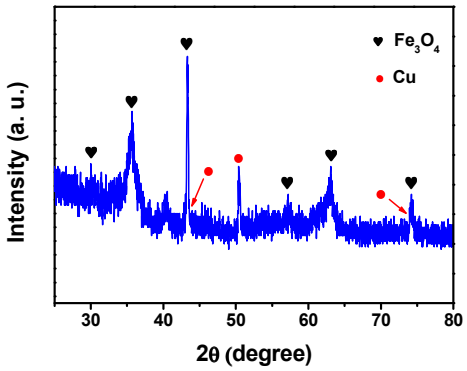

Fig. 1 Wide-angle XRD pattern of Cu/Fe_3O_4.

The successful preparation and their crystalline nature of the Cu/Fe_3O_4 nanospheres were attested by the typical wide-angle XRD pattern (see Fig. 1). The distinct peak appears at 2θ = 50.5^o corresponding to (200) crystal plane of metallic Cu,[42,43] which certifies the existence of zero-valent Cu in the composite. The other characteristic peaks of metal Cu at 2θ = 43.4^o and 74.2^o, attributed to (111), (220) crystal planes, were overlapped with that of (400), (533) crystal planes of Fe_3O_4.[44] In addition, in view of these characteristic peaks of Cu, it can be concluded that the crystalline structure of Cu was face-center cubic (fcc)[45,46] Meanwhile, the residue typical characteristic peaks of fcc lattice of spinel structure Fe_3O_4 were also distinctly appeared at 2θ = 30.1^o, 35.7^o, 57.2^o, and 62.9^o, assigned to (220), (311), (511), and (440) crystal planes, respectively.[47,48] In this light, the nanocomposite of Cu/Fe_3O_4 were successfully fabricated with the facile methodology.

The morphology, size, and texture properties of the as-synthesized Cu/Fe_3O_4 nanocomposites, as shown in Fig. 2, are obtained by the SEM and TEM analysis. For Fig. 2A, it can be clearly appreciated that the as-fabricated product was composed of large amounts of well-dispersed and uniform nanospheres and the average diameter of them were estimated to be approximately 100 nm. The higher-magnification SEM image (Fig. 2B) further revealed that the nanospheres have a sphere-like morphology and relatively rough surface, indicating that they consisted of many small secondary nanoparticles. The internal microstructure of the nanospheres was characterized by TEM. It could be clearly seen that the as-obtained well-defined nanospheres exhibited excellent dispersibility and uniformity (Fig. 2C). The higher-magnification TEM image (Fig. 2D) shows that the Cu/Fe_3O_4 nanospheres are assembled from hundreds of secondary nanoparticles as building blocks with average size of about 10 nm in diameter, leading to the formation of hierarchical structures with a sphere-like morphology and porous feature. Further, the HRTEM image inset in Fig. 2D clearly depicts the lattice fringes of Cu/Fe_3O_4. Among them, the lattice spacing of about 0.481 nm was coherent with the (111) plane of Fe_3O_4 crystal. The other lattice fringes with a lattice spacing of about 0.210 nm were assigned to the (111) plane of Cu crystal.[5,44] Combined the XRD results with that from SEM and TEM analysis, it can be easily concluded that the Cu/Fe_3O_4

nanocomposites were successfully prepared via one-pot hydrothermal reaction and were of sphere-like hierarchical structure.

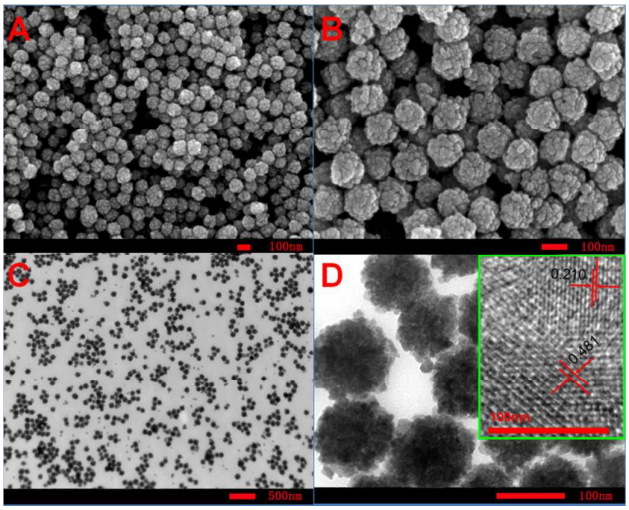

Fig. 2 SEM image (A), Higher-magnification SEM image (B), TEM image (C), Higher-magnification TEM image (D) and HRTEM image (inset) of Cu/Fe_3O_4.

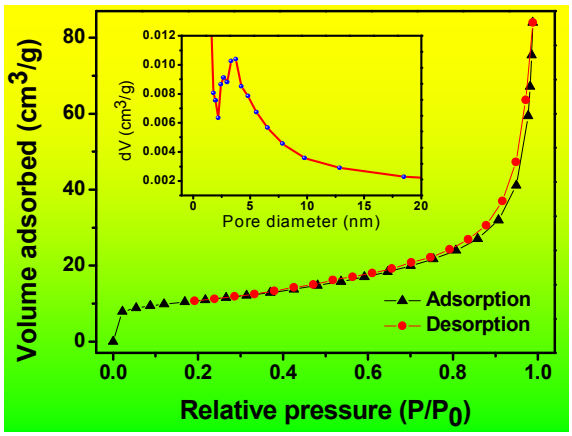

Fig. 3 N_2 adsorptione-desorption isotherms and (inset) the corresponding pore size distribution curve of Cu/Fe_3O_4.

On the other hand, the N_2 adsorption-desorption profiles obtained for the as-synthesized Cu/Fe_3O_4 nanospheres further proved the porosity of the product. As demonstrated in Fig. 3, which displays the N_2 adsorption-desorption isotherms and the corresponding BJH pore size distribution curve (inset in Fig. 3) for the Cu/Fe_3O_4 nanospheres. As depicted by the N_2 adsorption-desorption measurement (Fig. 3), the composite nanospheres exhibited a typical IV isotherm, suggesting the presence of interparticle and nonordered mesoporous network in the sample. Combined with the images of TEM, it can be concluded that the pores were derived from the random assembly of a large number of secondary nanoparticle building blocks in the formation process; and as a result, the pores were not very uniform, and the phenomenon was also reported by Ai et al.[28] According to the BJH pore distribution curve (inset in Fig. 3), the major pore size was estimated to be 3.73 nm. The BET surface area and pore volume of the Cu/Fe_3O_4 nanospheres were calculated to be 37.16 m^2/g and 0.13 cm^3/g, respectively, indicating the presence of mesopores in the hierarchical nanospheres, which agrees well with the SEM and TEM analysis results. Furthermore, considering the presence of mesopores, the hierarchical composite might be helpful for some potential applications like antibacterial, adsorption or catalysis domains.

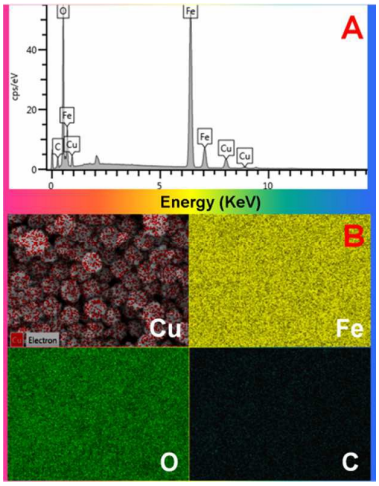

Fig. 4 EDS (A) and elemental mapping spectra (B) for Cu/Fe_3O_4.

The element composition and distribution of Cu/Fe_3O_4 nanospheres were verified by the EDS data and EDS mapping images. To obtain more accurate statistics, these characterizations were conducted through pressed pallet of products. As shown in Fig 4A, the EDS spectrum of Cu/Fe_3O_4 nanospheres confirmed the presence of Cu, Fe, C, and O elements, and validated the purity of the material. To further investigate the element distribution of the Cu/Fe_3O_4 nanospheres, the EDS mapping characterization was carried out. As shown in Fig. 4B, the different colour images represent element Cu, Fe, C, and O enriched areas of the sample, respectively. It was easy to speculate that all the elements distributed uniformly on the Cu/Fe_3O_4 nanocomposites.

To elucidate the surface properties and electronic structure of the product, the full-range XPS spectrum of the Cu/Fe_3O_4 nanospheres and high resolution spectrum of Cu element were conducted. Fig. 5A delineates the full-range XPS spectrum of the Cu/Fe_3O_4 nanospheres, from which no peaks of other elements except Cu, Fe, O, and C can be detected in the spectrum, well consistent with the EDS data. As for the high resolution XPS spectrum of Cu2p (Fig.5B), the apparent doublet peaks appeared at 952.9 and 932.9 eV were attributed to the $Cu2p_{1/2}$ and $Cu2p_{2/3}$ of metallic Cu,[49] respectively. That is, all the XPS results further proved the formation of the Cu/Fe_3O_4 nanocomposite and were well consistent with the results from XRD, TEM, and EDS, thus clearly indicating that the existence form of Cu in the composite was zero-valent and the Cu/Fe_3O_4 nanocomposite has been facilely fabricated by means of a short-time, green one-pot hydrothermal pathway

that avoided using toxic surfactant, organic solvent or reagents and tedious multiple steps.

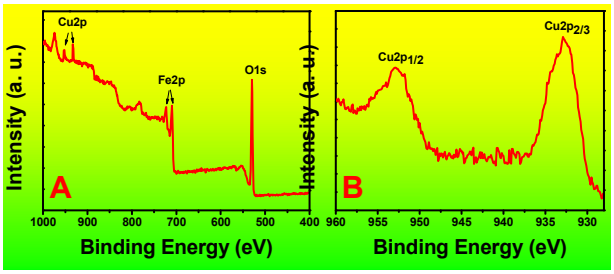

Fig. 5 (A) XPS survey spectra of Cu/Fe_3O_4; (B) High resolution core level spectra of Cu2p.

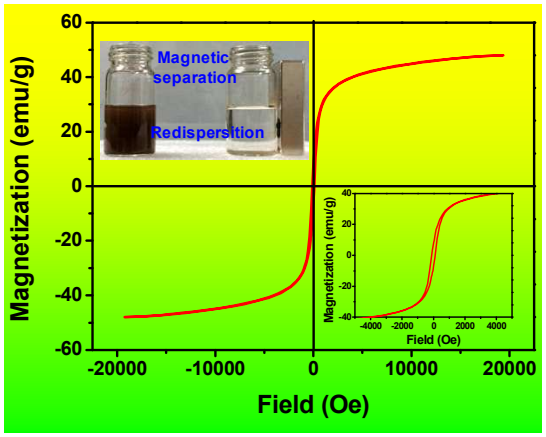

Fig. 6 Room temperature magnetization curve of Cu/Fe_3O_4.

Furthermore, the magnetic property of the as-prepared Cu/Fe_3O_4 nanocomposites was testified by the VSM analysis carried out in an applied magnetic field at room temperature with the field sweeping from -20 to 20 kOe. Fig. 6 portrays the magnetization curve of Cu/Fe_3O_4 nanospheres and the saturation magnetization value was measured to be 48.0 emu g^{-1}. Out of question, the as-prepared catalyst was capable of magnetic separation and recovery from aqueous system though the existence of coercivity (enlarged inset). As demonstrated in the photo inset in Fig. 6, the Cu/Fe_3O_4 nanospheres can be dispersed in water by vigorous shaking or sonication, resulting in a brown suspension. As discussed above, the as-prepared Cu/Fe_3O_4 nanospheres were sensitive to an external magnetic field, once a magnet was placed beside the vial, dispersed Cu/Fe_3O_4 in aqueous solution were quickly gathered to the side of the vial leaving the solution transparent, which was an intuitive proof of their magnetic nature. In addition, redispersion occurred quickly with a slight shaking when the magnet was removed away. All the results verified that the Cu/Fe_3O_4 nanospheres possess excellent magnetic responsivity and redispersibility, which were of significant importance in practical applications when used as a recyclable catalyst or adsorbent for water treatment.

Influences of Na_3Cit, urea and reaction time

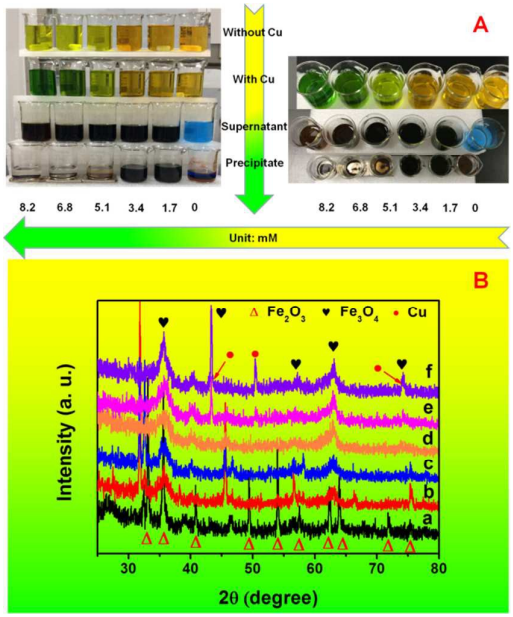

Fig. 7 (A) Photos of solutions under different conditions; (B) XRD patterns of the products with different dosage of Na_3Cit: (a) 0 mM, (b) 1.7 mM, (c) 3.4 mM, (d) 5.1 mM, (e) 6.8 mM, (f) 8.2 mM.

The effect of Na_3Cit dosage on the formation of Cu/Fe_3O_4 nanospheres was systematically investigated as follows from the viewpoints of their colour, phase structures and magnetization properties, respectively. As demonstrated in Fig. 7A, the solutions with different dosages of Na_3Cit and at different stages were put together for direct visual observation. Firstly, without the addition of Cu precursor, the colour of solution was changed gradually from orange, light yellow to yellow with the increase of Na_3Cit amount while keeping other parameters constant. After the addition of Cu precursor, the corresponding solution colour changed from orange, light green to green. The phenomenon can be explained by the stabilization effect of Na_3Cit. After the precursor solutions with different Na_3Cit amount reacted at 200 °C for 4 h in a Teflon-lined autoclave, the obtained supernatant and precipitate were collected severally. As shown in Fig. 7A, without addition of Na_3Cit, the supernatant colour was blue, revealing that Cu^{2+} was not reduced and the precipitate was red brown without magnetism. However, when the initial addition amount of Na_3Cit increased, the supernatant became transparent gradually. Meanwhile, the precipitate exhibited magnetic property while the amount of Na_3Cit higher than 1.5 g, and higher amount of Na_3Cit was added, the larger magnetic property was observed. The results can also be supported by the XRD data (Fig. 7B). Without Na_3Cit, as presented in Fig. 7B(a), apart from the peaks of Fe_2O_3, the characteristic peaks of Fe_3O_4 and Cu were not detected. Nevertheless, with the augment of initial Na_3Cit dosage, the peaks of Fe_2O_3 disappeared and the peaks of Fe_3O_4 and Cu^0 appeared and increased step by step. All the results discussed above proved that Na_3Cit in the reaction system played the role of stabilization and reductant for Fe^{3+} and Cu^{2+},

and the higher dosage was propitious to the formation of Cu/Fe_3O_4 with good crystallization. Hence, the optimal dosage of Na_3Cit was set to be 8.2 mM in the following reaction system.

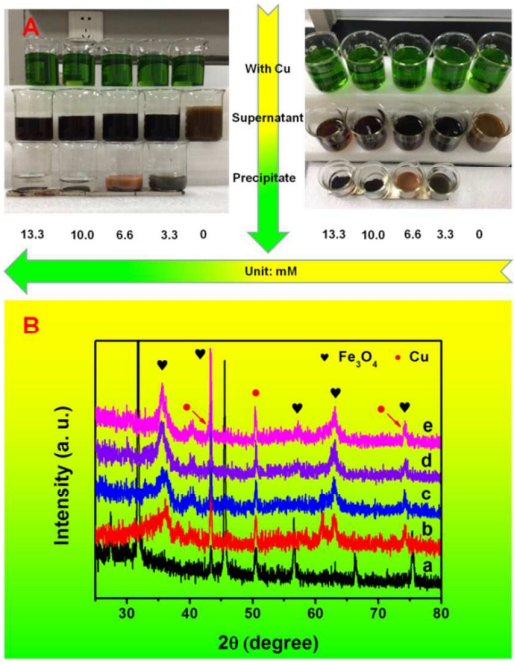

Fig. 8 (A) Photos of solutions under different conditions; (B) XRD patterns of the products with different dosage of urea: (a) 0 mM, (b) 3.3 mM, (c) 6.6 mM, (d) 10.0 mM, (e) 13.3 mM.

The effect of urea dosage on the formation of Cu/Fe_3O_4 was also explored. Similarly, in order to visualize the changes, the photos of solutions under different addition amount of urea and at different stages were displayed in Fig. 8A. It can be clearly seen that the colour of the solutions with different urea dosage were the same, i.e. they were all green. After reaction for 4 h at 200 ^{o}C in a Teflon-lined autoclave, we did not get precipitate except the turbid solution in the absence of urea. To figure out the composition of it, we directly dried the solution and used the acquisition to proceed the XRD analysis. On the other hand, the supernatant became clearer as the increase of urea dosage, and at the same time, the amount and magnetism of products obtained both increased. However, when the urea dosage was little, such as 0.2 g or 0.4 g, the amount of products decreased during washing process with water and the eluate was always coloured. To further figure out the influence of urea dosage from another point of view, XRD analysis was also carried out. As shown in Fig. 8B, the characteristic peak of Cu^0 at $2\theta = 50.5^o$ existed in all samples prepared with different amount of urea. But the typical peaks of Fe_2O_3 or Fe_3O_4 cannot be detected without the addition of urea. As the addition amount of urea increased, the typical peaks of Fe_3O_4 appeared and strengthened gradually. Therefore, we speculated that urea was indispensable during the formation of Cu/Fe_3O_4 through providing hydroxyl ions at high temperatures and the products obtained at little amount of urea were highly unstable.[50] As a result, the dosage of urea in our fabrication system was fixed to 10.0 mM.

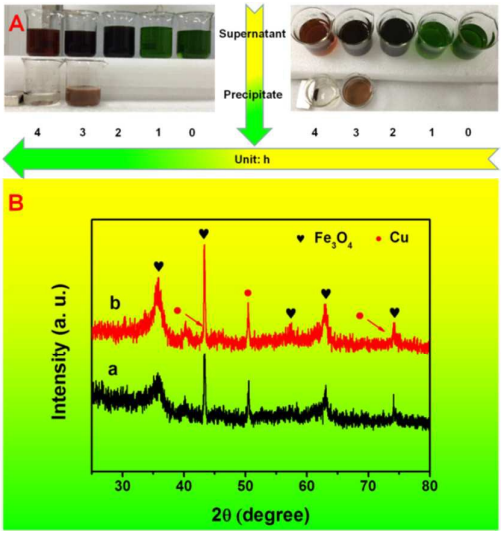

Fig. 9 (A) Photos of solutions under different conditions; (B) XRD patterns of the products under different reaction duration time: (a) 3 h, (b) 4 h.

To shed light on the formation process of Cu/Fe_3O_4 nanospheres, time-dependent experiments were also investigated carefully at 200 ^{o}C for different reaction intervals of 0 h, 1 h, 2 h, 3 h, and 4 h. As shown in Fig. 9, the pristine reaction solution was transparent and green in colour, which still unchanged after reaction for 1 hour at 200 ^{o}C. This indicates that no reaction happened in the system during the initial 1 h, although urea releases hydroxyl ions at such high temperature. It can be explained by the complex effect of Na_3Cit for iron ions.[51] After reaction for 2 h, the solution became turbid, but still no precipitate was acquired. When the reaction time increased to 3 h and 4 h, the precipitate was both obtained. However, the products obtained at 3 h of reaction time was not stable, which were decomposed during water washing process with coloured eluate and decreased amount. For another, it can be observed from the XRD results (Fig. 9B) that the crystallization and peaks intensity of Fe_3O_4 for 4 h were much better and stronger than that for 3 h. Accordingly, the reaction time of 4 h can be considered an optimum duration period.

Plausible formation mechanism of hierarchical Cu/Fe_3O_4 nanocomposites

Based on the above experimental observation and analysis, a plausible formation mechanism for the Cu/Fe_3O_4 nanospheres was proposed, and a schematic illustration for the formation process was demonstrated in Scheme 1. In our system, urea was served as an alkali source to release hydroxyl ions for the formation of Fe_2O_3, which further transformed into Fe_3O_4 at high temperatures. Na_3Cit acted as the eco-friendly complexing agent, stabilizer as well as reductant for

Fe^{3+} and Cu^{2+}. Under appropriate reaction conditions such as sufficiently high temperature (200 °C) and enough reaction time, the precursors would have come into being and undergone the reduction of Fe^{3+} and Cu^{2+}, the transmutation from Fe_2O_3 to Fe_3O_4 as well as the nucleation and growth processes to form tiny primary nanocrystals. The pre-synthesized nanocrystals will further aggregate into hierarchical nanospheres so as to minimization of interfacial energy.[51] Thus the whole formation process was accomplished through the gradual random assembly of nanocrystals and crystallization.

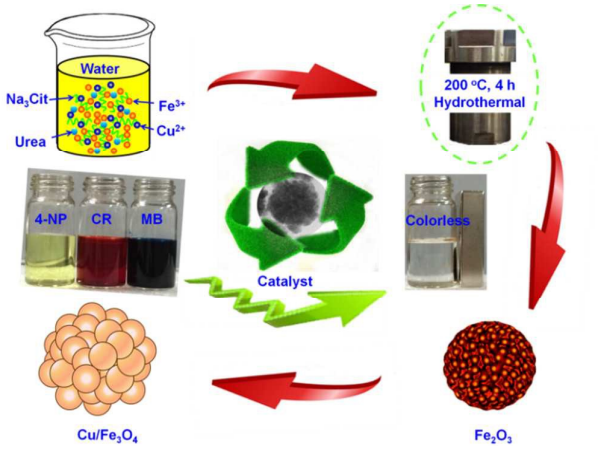

Scheme 1 Schematic illustration for the construction process and catalytic application of versatile Cu/Fe_3O_4 nanopspheres.

Catalytic reduction of various dyes

The reduction of heterocyclic aromatic compounds is commonly applied to study the catalytic performance of metal nanocatalysts. On the other side, considering the environmental and healthy concerns caused by the dyes and pigments mentioned above, we thus choose the reduction and decolouration of different dyes such as 4-NP, CR, and MB to evaluate the catalytic activity and versatility of as-prepared Cu/Fe_3O_4 nanospheres.

Firstly, we take the reduction of 4-NP as an example to introduce the catalytic reaction system. As demonstrated in Fig. 10A, the aqueous solution of 4-NP exhibited an absorbance peak at 317 nm. After the addition of $NaBH_4$, the peak immediately red-shifts to 400 nm due to formation 4-nitrophenolate ion under alkaline condition, and the colour changes from pale yellow to bright yellow (Fig. 10B). When Cu/Fe_3O_4 were added, the intensity of absorption peak at 400 nm gradually decreased in time; and meanwhile, a new absorption peak related to 4-AP appeared at 300 nm (Fig. 10C). Additionally, the UV-Vis spectra show an isosbestic point for the two absorption bands, indicating that the nitro compound was gradually converted to aminophenol without any side reactions.[52] After completion of the reaction, the peak at 400 nm was completely disappeared. Therefore, the reaction progress can be monitored by recording the UV-Vis absorption spectra of the reaction solution with respect to reaction time.

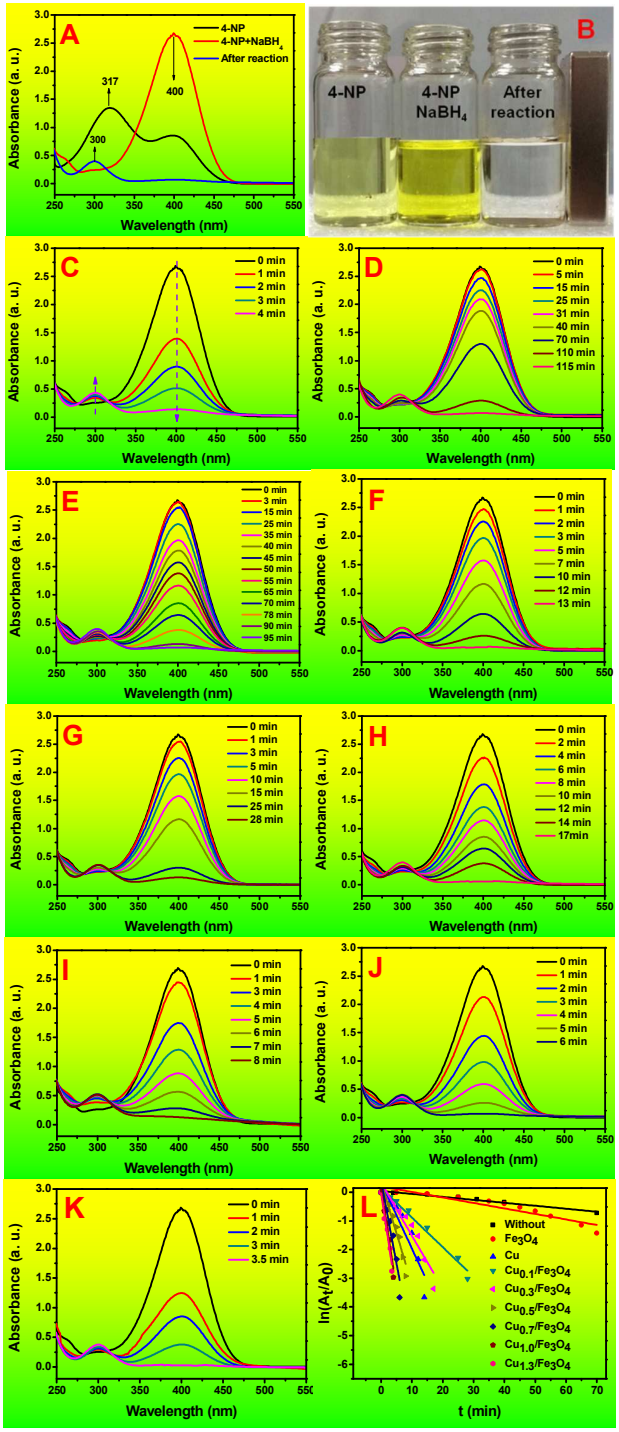

Fig. 10 UV-Vis absorption spectra (A) and color changes (B) of 4-NP under different conditions; Time-dependent UV-Vis absorption spectra in the presence of Cu/Fe_3O_4 (C), without catalyst (D), with Fe_3O_4 as catalyst (E), with Cu as catalyst (F); Time-dependent UV-Vis absorption spectra over Cu/Fe_3O_4 prepared at different dosage of Cu precursor: $Cu_{0.1}/Fe_3O_4$ (G), $Cu_{0.3}/Fe_3O_4$ (H), $Cu_{0.5}/Fe_3O_4$ (I), $Cu_{0.7}/Fe_3O_4$ (J), $Cu_{1.3}/Fe_3O_4$ (K). (L) The relationship between $\ln(A_t/A_0)$ and the reaction time at different conditions.

As shown in Fig. 10C, the reaction was completed within 4 min in the presence of Cu/Fe_3O_4. In addition, to prove the role of Cu/Fe_3O_4 composite played in the reaction system and the synergistic effect between Cu and Fe_3O_4, contrast experiment was also carried out, i.e., without catalyst, pure Fe_3O_4 or Cu synthesized with the same method as catalyst. It can be seen from Fig. 10D, E and F that it needed 115, 96, and 13 min for the reaction systems of without catalyst, with Fe_3O_4 or Cu as catalyst, respectively. Undoubtedly, it confirms that the catalytic activity was mainly due to the Cu species. More intriguingly, the catalytic performance of Cu/Fe_3O_4 composite was superior to pure Cu. The phenomenon can be explained by the following aspects: firstly, the existence of Fe_3O_4 support improved the dispersion of Cu, rendering it bigger active contact surface; secondly, there may exist synergistic effect between Cu and Fe_3O_4 in the composite. The detailed investigation of this phenomenon would be conducted in our further work.

On the other hand, considering the concentration of $NaBH_4$ was much higher than that of 4-NP, the reaction rate constant could be assumed to be independent of the concentration of $NaBH_4$, thus the pseudo-first order rate constant of the reaction *k* can be calculated from the equation $\ln(A_t/A_0)=kt$, where A_0 and A_t are the absorbance values of 4-NP initially and at time t, respectively. As shown in Fig. 10L, a good linear relationship between $\ln(A_t/A_0)$ and the reaction time was displayed, which was well consistent with pseudo-first order kinetics. Therefore, the apparent reaction rate constant *k* can be directly obtained from the slope of the linear plots. Moreover, the effect of initial addition amount of Cu precursor on the content of Cu in the composite and the catalytic properties of Cu/Fe_3O_4 was also investigated in details. As shown in Fig. 10C, G, H, I, J, K, with the increase of Cu precursor dosage, the time needed for the completion of the decoloration was decreased. Meanwhile, the content of Cu in the nanocomposite and reaction rate constant *k* both increased (Table 1 and Fig. 10L). Additionally, the XRD analysis results also verified this conclusion (Fig. S1). That is, the typical peak of Cu at $2\theta = 50.5^o$ increased with the augment of Cu precursor dosage. However, as the Cu precursor dose increased to 1.3 mM, the content of Cu in the nanocomposite and reaction rate constant *k* were not significantly increased. As such, it can be concluded that as the augment of Cu dosage, the exposed active site or surface increased and therefore facilitate the catalytic reaction. However, as the dosage of Cu increased to 1.3 mM, the Cu exposed to the surface of the nanosphere had reached its maximum, the improvement of catalytic performance was not obvious. This situation was also appeared in our previous work.[22] In this context, the optimal dose of Cu precursor in our system was 1.0 mM.

Table 1 The content of element in different composite and the corresponding kinetic data.

Entry	C	O	Fe	Cu	4-NP		CR		MR	
	wt%				k (min^{-1})	R^2	k (min^{-1})	R^2	k (min^{-1})	R^2
Without catalyst	0	0	0	0	0.01	0.97	0.03	0.99	0.07	0.97
Fe_3O_4	6.89	25.66	67.45	0	0.02	0.88	0.04	0.98	0.09	0.84
Cu	0	0	0	100	0.23	0.86	0.28	0.96	1.40	0.93
$Cu_{0.1}/Fe_3O_4$	7.27	26.34	65.70	0.69	0.10	0.98	0.10	0.93	1.08	0.75
$Cu_{0.3}/Fe_3O_4$	7.44	26.93	62.69	1.94	0.19	0.90	0.20	0.93	2.02	0.78
$Cu_{0.5}/Fe_3O_4$	7.79	26.85	61.32	4.04	0.36	0.91	0.30	0.92	3.82	0.90
$Cu_{0.7}/Fe_3O_4$	7.69	26.24	59.85	6.22	0.58	0.90	0.47	0.99	⋆	⋆
$Cu_{1.0}/Fe_3O_4$	7.60	26.06	59.26	7.08	0.69	0.94	1.23	0.88	⋆	⋆
$Cu_{1.3}/Fe_3O_4$	7.76	26.13	58.79	7.32	0.71	0.95	1.48	0.98	⋆	⋆

All the content were obtained from the EDS analysis.

⋆ Meaning that the reaction was too fast to acquire the accurate reaction data.

Similarly, the catalytic performance of Cu/Fe_3O_4 for the reduction of CR and MB was also explored. To obtain accurate data by means of UV-Vis spectroscopy based on Lambert-Beer Law, the concentrations of CR and MB and the amount of catalyst were all decreased compared to the reaction system of 4-NP, and the time-dependent UV-Vis absorption spectra and reaction kinetic data were presented in Fig. S2, S3 and Table 1. In the presence of Cu/Fe_3O_4, it just required 3 min and 10 s to completely reduce CR and MB respectively, whereas it took 75 and 32 min to reduce CR and MB in the absence of catalyst. All the results indicated that the Cu/Fe_3O_4 nanocomposites possess universal catalytic properties for the degradation of organic dyes under aqueous conditions.

Stability and recyclability of Cu/Fe_3O_4 nanocatalysts

The stability of the active ingredient is extremely important in heterogeneous catalysis. Hence, the leaching test was conducted using the reduction of 4-NP as the model reaction. Given the superparamagnetism discussed above, in the duplicate reaction, the catalyst Cu/Fe_3O_4 was separated by magnetic separation after 1 min and then the filtrate was further conducted for studying the continuing activity in the reaction system. As shown in Fig. 11, no further conversion of dyes could be detected in the filtrate, indicating that the active species of Cu was stable in the nanocomposite.

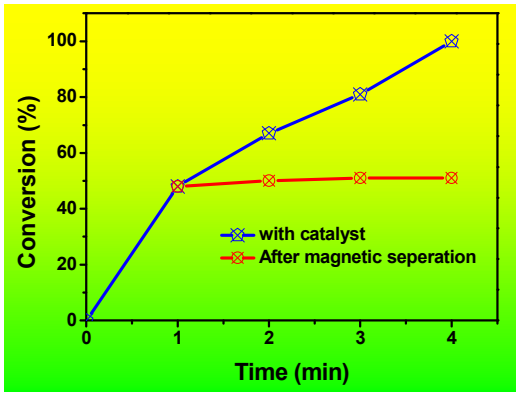

Fig. 11 Stability testing of Cu constituent in Cu/Fe_3O_4.

From another point of view, the recycling experiment also testified the stability and reusability of Cu/Fe_3O_4. After each cycle, the catalyst was collected from the reaction system by a magnet. Hereafter, the collected catalysts were rinsed with de-ionized water, dried, and reused as the catalyst for another run under the identical reaction condition. As presented in Fig. 12, the conversions of 4-NP, MB, and CR were still higher than 98% even after six successive cycles; further, the results from XRD demonstrated that no obvious changes was detected before and after recycled for six times (Fig. S4), clearly indicating that the Cu/Fe_3O_4 nanocomposite possessed appealing stability and reusability. In this sense, the presented hierarchical nanocomposites with high catalytic activity, excellent stability and recyclability may find promising potential applications in the domains of biomedicine and wastewater treatment.

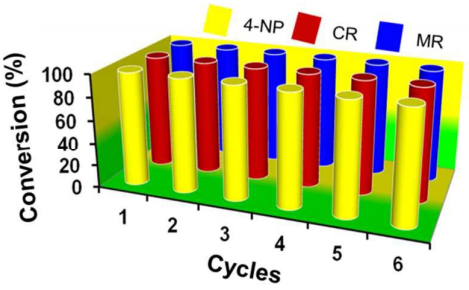

Fig. 12 Recycling catalytic performance of Cu/Fe_3O_4 for the various organic dyes.

Conclusions

In summary, we have demonstrated a facile, short-time, economical, and eco-friendly fabrication method of hierarchical Cu/Fe_3O_4 nanospheres through a simple hydrothermal method by mixing $FeCl_3 \cdot 6H_2O$, Na_3Cit, urea and $Cu(NO_3)_2 \cdot 3H_2O$. The synthesis parameters and time dependent experiments were constructed to investigate the synthesis procedure of Cu/Fe_3O_4, which indicated that the mesoporous hierarchical nanospheres were formed via the gradual random assembly of tiny secondary nanoparticles and crystallization. The saturated magnetization of the Cu/Fe_3O_4 nanospheres was 48.0 emu g^{-1} at room temperature, which endowed them with easy separation and recovery properties by simply applying an external magnet. More importantly, the nanocomposites exhibited excellent versatile catalytic performance for the degradation of 4-NP (4 min), CR (3 min), MB (10 s), and good stability as well as recyclability (reused at least 6 times). On the basis of the multiple advantages, this hierarchical Cu/Fe_3O_4 nanospheres can be extended to adsorption, biological applications and fine chemical synthesis and so on.

Acknowledgements

Financial support from the National Natural Science Foundation of China (21446001), the Program for Liaoning Innovative Research Team in University (LT2013012) and the Program for Liaoning Excellent Talents in University (LJQ2014056) is highly appreciated.

Notes and references

1 M. R. Hoffmann, S. T. Martin, W. Choi, D. W. Bahnemann, Chem. Rev., 1995, **95**, 69.
2 T. Bhowmik, M. K. Kundu and S. Barman, RSC Adv., 2015, **5**, 38760.
3 H. Zhang, D. Chen, X. J. Lv, Y. Wang, H. X. Chang and J. H. Li, Environ. Sci. Technol., 2010, **44**, 1107.
4 B. Manu and S. Chaudhari, Bioresour. Technol., 2002, **82**, 225.
5 W. J. Liu, K. Tian, H. Jiang and H. Q. Yu, Green Chem., 2014, **16**, 4198.
6 M. Nemanashi and R. Meijboom, J. Colloid and Interface Sci., 2013, **389**, 260.
7 Z. Z. Wang, S. R. Zhai, B. Zhai, Z. Y. Xiao and Q. D. An, Prog. Chem., 2014, **26(2/3)**, 234.
8 A. Mignani, S. Fazzini, B. Ballarin, E. Boanini, M. C. Cassani, C. Maccato, D. Barreca and D. Nanni, RSC Adv., 2015, **5**, 9600.
9 Z. Z. Wang, S. R. Zhai, B. Zhai, Z. Y. Xiao, F. Zhang and Q. D. An, New J. Chem., 2014, **38**, 3999.
10 P. S. Mueller, C. P. Parker and S. C. Larsen, Micropor. Mesopor. Mat., 2015, **204**, 173.
11 J. Fernandez, J. Bandara, A. Lopez, P. Buffat and J. Kiwi, Langmuir, 1999, **15**, 185.
12 N. Riaz, F. K. Chong, B. K. Dutta, Z. B. Man, M. S. Khan and E. Nurlaela, Chem. Eng. J., 2012, **185-186**, 108.
13 A. R. Khataee, M. N. Pons and O. Zahraa, J. Hazard. Mater., 2009, **168**, 451.
14 S. Pany, K. M. Parida and B. Naik, RSC Adv., 2013, **3**, 4976.
15 S. K. Samantaray, P. Mohapatra and K. Parida, J. Mol.Catal. A, 2003, **198**, 277.

16 X. Chen, Z. F. Zheng, X. B. Ke, E. Jaatinen, T. F. Xie, D. J. Wang, C. Guo, J. C. Zhao and H. Y. Zhu, Green Chem., 2010, **12**, 414.
17 Z. G. Xiong, L. L. Zhang, J. Z. Ma and X. S. Zhao, Chem. Commun., 2010, **46**, 6099.
18 F. J. Cervantes, A. Garcia-Espinosa, M. A. Moreno-Reynosa and J. R. Rangel-Mendez, Catal. Sci. Technol., 2010, **44**, 1747.
19 S. Ghorai, A. Sarkar, M. Raoufi, A. B. Panda, H. Schönherr and S. Pal, ACS Appl. Mater. Inter., 2014, **6**, 4766.
20 P. F. Ji, J. L. Zhang, F. Chen and M. Anpo, Appl. Catal. B: Environ., 2009, **85**, 148.
21 R. Rajesh, E. Sujanthi, S. S. Kumar and R. Venkatesan, Phys. Chem. Chem. Phys., 2015, **17**, 11329.
22 Z. Z. Wang, S. R. Zhai, B. Zhai and Q. D. An, Eur. J. Inorg. Chem., 2015, **2015**, 1692.
23 J. Li, C. Y. Liu and Y. Liu, J. Mater. Chem., 2012, **22**, 8426.
24 A. Gangula, R. Podila, R. M, L. Karanam, C. Janardhana and A. M. Rao, Langmuir, 2011, **27**, 15268.
25 M. Shokouhimehr, J. E. Lee, S. I. Han and T. Hyeon, Chem. Commun., 2013, **49**, 4779.
26 A. Tao, P. Sinsermsuksakul and P. D. Yang, Angew. Chem. Int. Ed. 2006, **45**, 4597.
27 A. W. Sanders, D. A. Routenberg, B. J. Wiley, Y. Xia, E. R. Dufresne and M. A. Reed, Nano Lett., 2006, **6**, 1822.
28 L. H. Ai, C. M. Zeng and Q. M. Wang, Catal. Commun., 2011, **14**, 68.
29 H. Lee, H. Kim, T. J. Choi, H. W. Park and J. Y. Chang, Chem. Commun., 2015, **51**, 9805.
30 X. Q. Cheng, M. Liu, A. F. Zhang, S. Hu, C. S. Song, G. L. Zhang and X. W. Guo, Nanoscale, 2015, **7**, 9738.
31 G. W. Wang, D. Kundu and H. Uyama, J. Colloid and Interf. Sci., 2015, **451**, 184.
32 J. Gao, J. Xu, S. X. Wen, J. Hu and H. L. Liu, Micropor. Mesopor. Mater., 2015, **207**, 149.
33 B. K. Ghosh, S. Hazra, B. Naik and N. N. Ghosh, Powder Technol., 2015, **269**, 371.
34 B. Naik, S. Hazra, V. S. Prasad and N. N. Ghosh, Catal. Commun., 2011, **12**, 1104.
35 Z. Z. Wang, S. R. Zhai, F. Zhang, Z. Y. Xiao, B. Zhai and Q. D. An, J. Sol-Gel Sci. Technol., 2015, **73**, 299.
36 F. P. Dong, W. P. Guo and C. S. Ha. J. Nanopart. Res., 2012, **14**, 1303.
37 T. Zeng, X. L. Zhang, S. H. Wang, Y. R. Ma, H. Y. Niu and Y. Q. Cai, J. Mater. Chem. A, 2013, **1**, 11641.
38 W. C. Guo, Q. Wang, G. Wang, M. Yang, W. J. Dong and J. Yu, Chem. Asian J., 2013, **8**, 1160.
39 Y. Y. Li, D. Y. Yuan, M. J. Dong, Z. H. Chai and Q. Fu. Guo, Langmuir, 2013, **29**, 11770.
40 D. H. Zhang, G. D. Li, J. X. Li and J. S. Chen, Chem. Commun., 2008, 3414.
41 T. Wang, W. C. Yang, T. T. Song, C. F. Li, L. Y. Zhang, H. Y. Wang and L. Y. Chai, RSC Adv., 2015, **5**, 50011.
42 S. Y. Gao, X. X. Jia, J. M. Yang and X. J. Wei, J. Mater. Chem., 2012, **22**, 21733.
43 P. Deka, R. C. Deka and P. Bharali, New J. Chem., 2014, **38**, 1789.
44 M. Y. Tang, S. Zhang, X. X. Li, X. B. Pang and H. X. Qiu, Mater. Chem. Phys., 2014, **148**, 639.
45 Y. L. Zhang, W. W. Yan, Z. M. Sun, X. C. Li and J. P. Gao, RSC Adv., 2014, **4**, 38040.
46 C. C. Yeh, P. R. Wu and D. H. Chen, Mater. Lett., 2014, **136**, 274.
47 Z. U. Rahmana, Y. L. Dong, L. Su, Y. H. Ma, H. J. Zhang and X. G. Chen, Chem. Eng. J., 2013, **222**, 382.
48 G. Dodi, D. Hritcu, G. Lisa and M. I. Popa, Chem. Eng. J., 2012, **203**, 130.
49 R. Liu, Y. L. Guo, G. Odusote, F. L. Qu and R. D. Priestley, ACS Appl. Mater. Interfaces., 2013, **5**, 9167.
50 B. F. Zou, Y. F. Liu and Y. Q. Wang, RSC Adv., 2013, **3**, 23327.
51 D. J. Kang, X. L. Yu, M. F. Ge and W. G. Song, Micropo. Mesopor. Mat., 2015, **207**, 170.
52 B. J. Lee, J. C. Park and H. Song, Adv. Mater., 2008, **20**, 1523.

Graphical Abstract:

A novel monodispersed hierarchical nanocomposite catalyst, i.e. Cu/Fe_3O_4, aiming for efficient degradation of traditional dyes, was successfully synthesized through a short-time, facile, eco-friendly hydrothermal method.